

## Article

# Precious-Metal Mineralization and Formation Conditions of the Biche-Kadyr-Oos Epithermal Au-Ag Ore Occurrence (Eastern Sayan, Russia)

Renat V. Kuzhuget <sup>1,\*</sup>, Natalia N. Ankusheva <sup>1,2,3,\*</sup> , Ailai K. Hertek <sup>1</sup>, Yuri A. Kalinin <sup>4</sup>, Bulat B. Damdinov <sup>5</sup> , Franco Pirajno <sup>6</sup>, Yuri V. Butanaev <sup>1</sup>, Nadezhda V. Suge-Maadyr <sup>1</sup> and Sholban N. Soldup <sup>1</sup>

<sup>1</sup> Tuvinian Institute for Exploration of Natural Resources of Siberian Branch of RAS (TuvIENR SB RAS), 667007 Kyzyl, Russia; ajlan@mail.ru (A.K.H.); jyra3@mail.ru (Y.V.B.); nadu.suge@mail.ru (N.V.S.-M.); sholkaka85@mail.ru (S.N.S.)

<sup>2</sup> South Urals Federal Research Center of Mineralogy and Geoecology UB RAS, Institute of Mineralogy, 456317 Miass, Russia

<sup>3</sup> Geological Faculty, South Urals State University, 456314 Miass, Russia

<sup>4</sup> Sobolev Institute of Geology and Mineralogy SB RAS, 630090 Novosibirsk, Russia; yuri.a.kalinin@mail.ru

<sup>5</sup> Dobretsov Geological Institute SB RAS, 670047 Ulan-Ude, Russia; damdinov@mail.ru

<sup>6</sup> Centre for Exploration Targeting, University of Western Australia, Perth, WA 6009, Australia; franco.pirajno@uwa.edu.au

\* Correspondence: rkuzhuget@mail.ru (R.V.K.); ankusheva@mail.ru (N.N.A.)

**Abstract:** The Biche-Kadyr-Oos epithermal Au-Ag ore occurrence is a prospective object in the Ak-Sug porphyry copper ore cluster (Eastern Sayan) in the northern part of the Central Asian orogenic belt (CAOB). The mineralization consists of gold-sulfide-quartz and gold-polysulfide-carbonate-quartz veins with argillic zones in the Lower Cambrian volcanic-sedimentary rocks. The origin of the Au-Ag ore occurrence is still debatable. To determine the origin, we examined the mineralogical and geochemical features, conditions of formation, and fluid sources of the Biche-Kadyr-Oos ore. A mineralogical and geochemical investigation outlines three stages of mineral formation: early argillic stage; gold-sulfide-quartz stage with pyrite, marcasite, pyrrhotite, arsenopyrite, chalcopyrite, less frequently sphalerite, hessite, gold, and electrum; and late gold-polysulfide-carbonate-quartz stage with gold, electrum, Hg-electrum, Se-acanthite, Se-galena, bornite, tennantite, tetrahedrite, hessite, tellurobismuthite, bismuthinite, matildite, jamesonite, ourayite, native Bi, and barite. Fluid inclusion study (thermometry, Raman spectroscopy) in quartz and mineral thermometry (electrum and sphalerite paragenesis) determined that ore veins were formed at P~0.5 kbar from CO<sub>2</sub>-water Na-K-chloride fluid (4.9–9.6 wt % NaCl eqv) and temperatures from 300 to 200 °C (early gold-sulfide-quartz veins at 300–230 °C, and late gold-polysulfide-carbonate-quartz veins at 290–200 °C) and variations in  $f_{O_2}$ ,  $f_{S_2}$ ,  $f_{Se_2}$  and  $f_{Te_2}$ . The S isotopic composition in sulfides and  $\delta^{34}S_{H_2S}$  values of the fluid are +1.3‰ and +4.7‰, respectively, (T = 300–275 °C) indicating magmatic S in ore formation. The oxygen isotope data indicate that during the formation of veins, the magmatic fluid mixed with meteoric water ( $\delta^{18}O_{fluid}$  is from +3.4 to +6.4‰). The isotopic data that were obtained combined with mineralogical and geochemical features and conditions of ore formation indicate the similarity of Biche-Kadyr-Oos ore occurrence with epithermal Au-Ag deposits of intermediate sulfidation (IS) type. The presence of epithermal Au-Ag mineralization of the Biche-Kadyr-Oos IS type in ore cluster of the Ak-Sug Cu-Au-Mo porphyry deposit indicates the existence of a single porphyry-epithermal ore-magmatic system.

**Keywords:** native gold; Au-Ag epithermal mineralization; quartz; fluid inclusions; stable isotopes; Tuva



**Citation:** Kuzhuget, R.V.; Ankusheva, N.N.; Hertek, A.K.; Kalinin, Y.A.; Damdinov, B.B.; Pirajno, F.; Butanaev, Y.V.; Suge-Maadyr, N.V.; Soldup, S.N. Precious-Metal Mineralization and Formation Conditions of the Biche-Kadyr-Oos Epithermal Au-Ag Ore Occurrence (Eastern Sayan, Russia). *Minerals* **2023**, *13*, 1529. <https://doi.org/10.3390/min13121529>

Academic Editors: Gülcan Bozkaya, David Banks and Evgeniy Naumov

Received: 18 September 2023

Revised: 24 November 2023

Accepted: 2 December 2023

Published: 8 December 2023



**Copyright:** © 2023 by the authors. Licensee MDPI, Basel, Switzerland. This article is an open access article distributed under the terms and conditions of the Creative Commons Attribution (CC BY) license (<https://creativecommons.org/licenses/by/4.0/>).

## 1. Introduction

Porphyry Cu-Au-Mo deposits were identified on the Tuva segment of the Central Asian orogenic belt (CAOB), where the largest are the Ak-Sug and Kyzzyk-Chadr deposits in Eastern Tuva, with significant reserves and resources [1,2]. The porphyry Cu-Au-Mo deposits are associated with Early-Middle Cambrian calcareous-alkaline porphyry intrusions [3–5].

Spatially and genetically, porphyry Cu deposits can be associated with Au-Ag epithermal gold-sulfide and other deposits that vertically succeed each other and form a single porphyry-epithermal ore-magmatic system [6–9]. Prospecting and exploration of new deposits at the periphery of the same ore clusters are of great interest. Many Cu porphyry ore occurrences (Kadyroy, Grebeshkovy, Dashtyg, Biche-Kadyr-Oos, etc.) were identified in the Ak-Sug ore cluster (Eastern Sayan). Biche-Kadyr-Oos veined ore occurrence is one of the potential prospects for native Au. The genesis is still debatable, and mineralogical and geochemical features have not yet been sufficiently examined.

The Biche-Kadyr-Oos occurrence is located in volcanic-sedimentary rocks of the Kham-sari Formation ( $C_1$ ). The diorite and gabbro-diorite intrusions of the Ak-Sug complex ( $C_{1ak}$ ) cut the volcano-sedimentary rocks. The Biche-Kadyr-Oos ore occurrence is believed to be the result of both VMS and veinlet-disseminated Cu porphyry mineralization [1]. It is assumed that the vein zones of this ore occurrence are developed over an undiscovered object of stockwork Au-Mo-Cu-porphyry mineralization (the Ak-Sug deposit type).

The aim of this paper is to examine the mineralogical and geochemical peculiarities and conditions of the formation of the Biche-Kadyr-Oos ore and to identify the ore-formational type.

## 2. Geological Setting

The Tuva segment is located in the northern part of the CAO. This region is bordered by the Caledonian structures of the Western Sayan in the west. The Early Baikal and Early Caledonian structures of the Eastern Sayan on the southern boundary of the Siberian craton are in the north and northeast. The N boundary of the Precambrian Tuva-Mongolian microcontinent (the largest tectonic block of the CAO) is located at the east and southeast borders. The Early Caledonides of the Ozernaya island-arc zone of Western Mongolia are in the south (Figure 1).

The Tuva segment of the CAO is an accretional and collisional structure formed during the geodynamic evolution and closure of the Paleasian Ocean [10–12]. The Eastern Tuva backarc, Sayano-Tuva forearc, and Tannuola-Khamsarin island-arc zones are distinguished within the Tuva segment. The Tannuol-Khamsarin island-arc zone is subdivided into the Khamsarin, Ondum, and Tannuola zones. The geological and tectonic structures in the region developed over a long time in stages of successive changes in geodynamic regimes (oceanic with primitive island-arc complexes ~1000–600 Ma, island-arc—570–518 Ma, accretion-collision—510–450 Ma, etc.) [13]. Each stage included particular magmatic and ore formations.

The evolution of the Tuva segment of the CAO provides the formation of the Upper Proterozoic and Paleozoic rock complexes in the region: island-arc volcano-plutonic assemblages of the ophiolite belts, the sedimentary and basement rocks of the microcontinent [10–12].

The Biche-Kadyr-Oos ore occurrence of the Ak-Sug Cu-Au-Mo porphyry ore cluster is located on the Eastern Sayan in the Vendian and Early Cambrian island-arc complexes of the Khamsarin subzone of the Tannuola-Khamsarin island-arc zone formed during the Paleasian ocean subduction [11]. The Kandat fault zone divides the Khamsarin subzone and the Kizir (East Sayan) structural-facial zone.

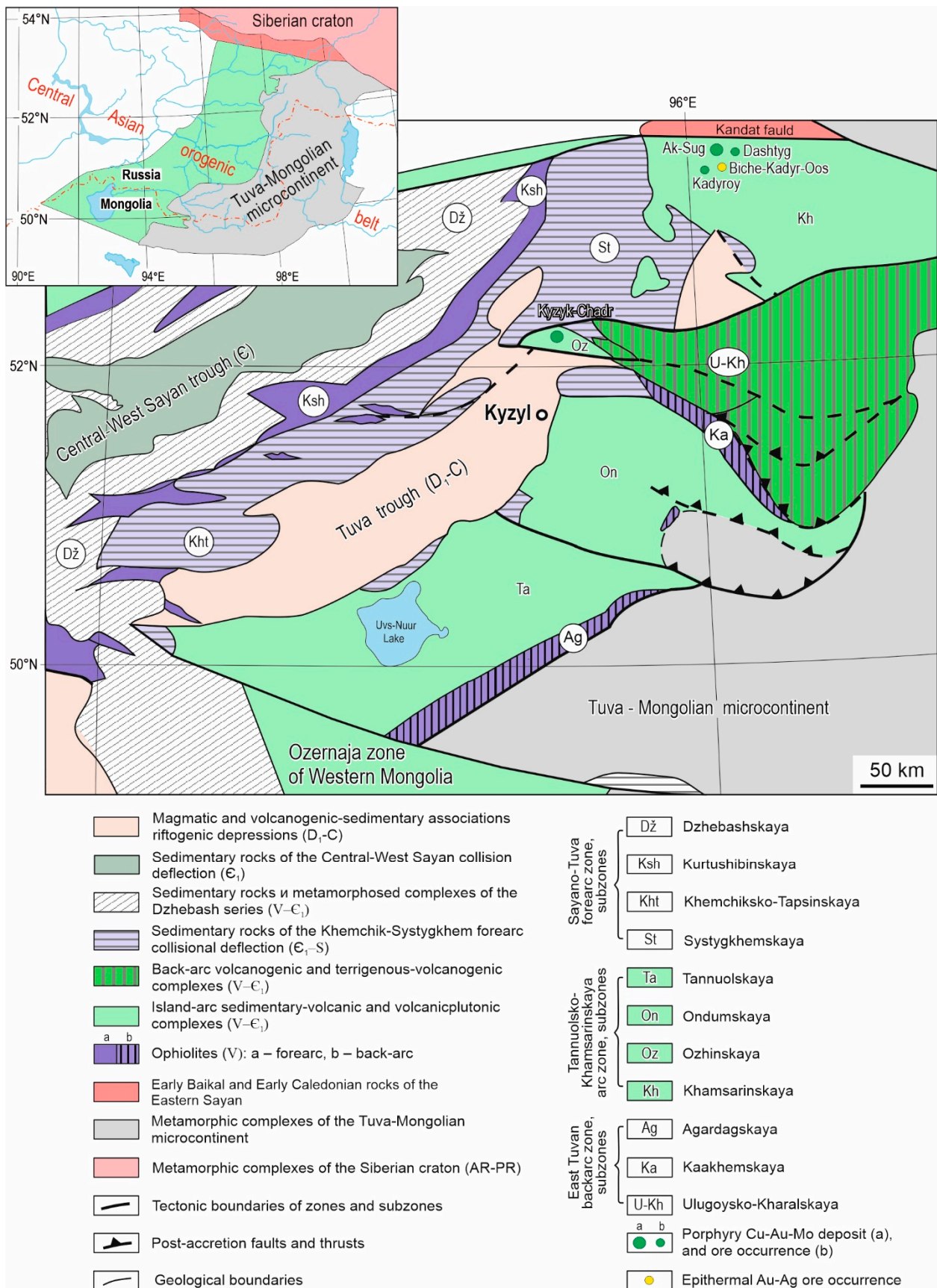


**Figure 1.** Geological and tectonic scheme of the Tuva segment of the CAOB (according to A.A. Mongush [14]).

The ore occurrence was discovered in 1963 during a 1:200,000 (1 sm–2 km) geological survey in the Biche-Kadyr-Oos River headwaters [2]. Overlapping trough faults (Dashtygoy, Kadyroy, etc.) formed by volcano-sedimentary rocks of the Khamsari Formation ( $\mathcal{E}_1$ ) border the southern flank of the Kandat fault. Massifs and stocks of porphyry granitoid intrusions of the Middle-Upper Paleozoic are localized in the frames of trough faults and along the plicative structures of sublatitudinal, northwestern, and northeastern directions.

The mineralization is characterized by different types of ore mineralization and is controlled by intrusive bodies or tectonic zones. In the Ak-Sug ore cluster, porphyry Cu-type deposits and ore occurrences and single epithermal Au-Ag ore occurrences are formed (Figure 1).

The age of Ak-Sug Cu-Au-Mo porphyry (the U-Pb dating (of Zr) of ore-bearing intrusions is  $515 \pm 4$  to  $499 \pm 6$  Ma [3]; Re-Os dating (of molybdenite) is 518, 517, 516, and 511 Ma [4,5]) suggests that the Cu-Au-Mo porphyry mineralization was formed during the geodynamic change from island arc (570–518 Ma) to accretionary-collision (510–450 Ma).

The Biche-Kadyr-Oos ore occurrence is confined to the junction area of Precambrian and Early Caledonian structures, in hydrothermally altered volcanic and sedimentary rocks of the Khamsara suite ( $\mathcal{E}_1$ ) with differently oriented tectonic faults of the Cheldezrik Fault (branch of the Kandat fault), intrusive bodies of diorite and gabbro-diorite bodies of the Tannuola complex ( $\mathcal{E}_{1tn}$ ), and small stocks of porphyry granites of the Ak-Sug complex ( $\mathcal{E}_{1ak}$ ). The mineralization is confined to the syn-ore SW tectonic faults (Figures 1 and 2).

Gold mineralization is represented by quartz (more than 20) and quartz-carbonate (more than 15) veins in the volcanic-sedimentary rocks of the Khamsar formation ( $\mathcal{E}_1$ ) over an area of about 1 km<sup>2</sup>. The volcanogenic-sedimentary Khamsar Formation ( $\mathcal{E}_1$ ) is composed of andesite, andesibasalt porphyrites and tuffs, with interlayers of rhyolites, shales, and sandstones. Basalts and andesibasalts consist of plagioclase and pyroxene, which are strongly altered. Pyroxene in porphyritic outcrops is represented by augite, which is most often indeterminate due to complete replacement by secondary minerals. Rhyolites in phenocrysts contain quartz and oligoclase or oligoclase. The thickness of the Lower Khamsarinsky Subformation is more than 1100 m.

According to a geological survey in 1963–1965, the ore occurrence included three veined zones: Zapadnaya, Shirotnaya, and Tsentralnaya. They are located along the NE or SW and are 500 m away from one another. The zones are 5–30 m thick and 150–300 m long. Each zone contains up to 10 ore veins 0.2–4.0 m thick and 10–80 m long (Figure 2).

The *Shirotnaya* veined zone is composed of gold-sulfide-quartz and gold-polysulfide-carbonate-quartz veins up to 10 m thick and up to 150 m long in the view of crushing zones in plagioclase-pyroxene porphyries from 30 to 40 cm to 1 m thick, with a vertical or inclined (70–80°) dip to NE-NW.

Gold-sulfide-quartz veins have pyrite-arsenopyrite-chalcopyrite composition with rare Au segregation. Gold-polysulfide-carbonate-quartz veins with ankerite and siderite are crosscutting and contain galena, sphalerite, chalcopyrite, fahlores, and gold.

The *Tsentralnaya* veined zone is composed of isolated early gold-sulfide-quartz veins deposited in a SW fault zone with a vertical or steep SW dip. The veins are discontinuous along the strike with narrowing and wedges in the flanks. They are from 0.2 to 1.4 m thick and up to 300 m long. Ore mineralization includes pyrite, chalcopyrite, fahlores, bornite, and Au. The veined zone is characterized by intense hydrothermal alteration of host volcano-sedimentary rocks and granite-porphyry intrusion of the Ak-Sug complex ( $\mathcal{E}_{1ak}$ ).

The *Zapadnaya* veined zone is localized in volcano-sedimentary rocks and less frequently in diorite-porphyries and comprises lens-shaped silicified and pyritized rocks and sometimes veins with chalcopyrite. The zone is up to 200 m long and includes up to 8 lens-like bodies up to 3–4 m thick and up to 50–60 m long. The ore minerals are pyrite and less frequently chalcopyrite. Most likely, the ore veins here are located hypsometrically below the silicified and pyritized rocks.

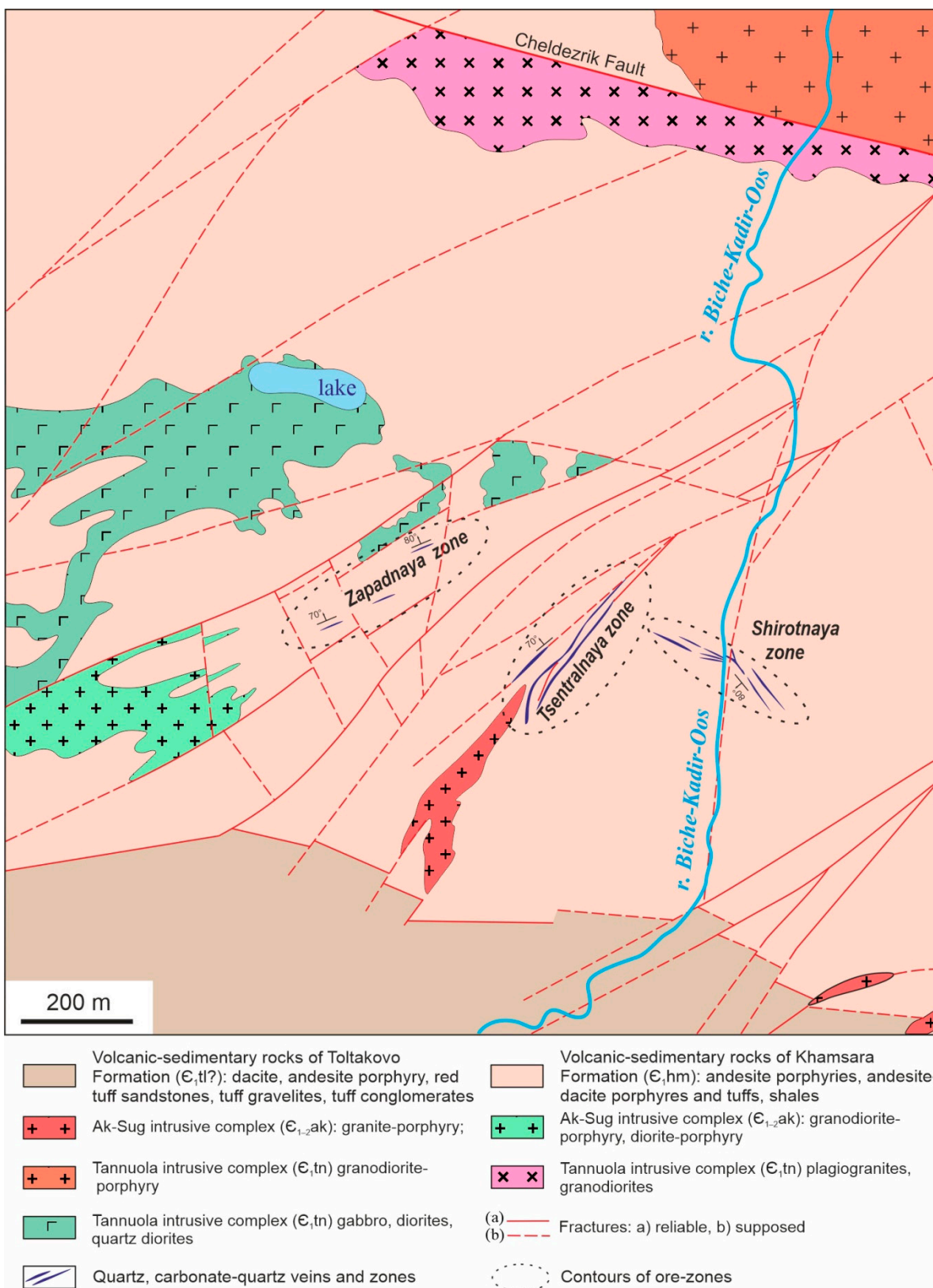


Figure 2. Geological structure of the Biche-Kadyr-Oos ore occurrence [1].

Gold-sulfide-quartz and gold-polysulfide-carbonate-quartz veins are accompanied by sheet-shaped bodies of hydrothermally altered quartz-sericite-kaolinite rocks. The Zapadnaya zone of hydrothermal alteration complies with metasomatites formed in the fringes

of gold-sulfide-quartz and gold-polysulfide-carbonate-quartz veins of the Shirotnaya and Tsentralnaya zones. In general, hydrothermally altered quartz-kaolinite-sericite rocks form zones 20–50 m thick and up to 400 m long [1]. Ore mineralization in veins is disseminated, rarely nest-like. According to [1], the contents of valuable components in mineralized rocks and ore veins are as follows: Cu 1%–1.5%, Zn 1%–1.5%, Ag up to 183 ppm (average value of 25.4 ppm), and Au up to 10 ppm (average value of 2.11 ppm).

### 3. Methods

Samples of ores and hydrothermally altered rocks were collected from the surface of the ore zone from outcrops and exploration trenches. We studied polished sections on Olympus BX41 and POLAM P-213M microscopes at Tuvian Institute for Exploration of Natural Resources SB RAS (Kyzyl, Russia). The chemical composition of minerals was determined using a MIRA 3 LMU SEM (Tescan Orsay Holding, Brno, Czechia) with INCA Energy 450 + XMax 80 and INCA Wave 500 microanalysis systems (Oxford Instruments Nanoanalysis Ltd., Oxford, UK) (Institute of Geology and Mineralogy SB RAS, Novosibirsk, Russia). The compositions of native gold and other minerals were examined at the accelerating voltage of 20 kV, an electron beam current of 1.5 nA, and live acquisition time of spectra of 30 s. The following X-rays were selected: K series for Fe, Cu, and Ni, and L series for Pd, Au, Ag, As, Te, Se, Bi, Sb, and Hg. As the standards, we used FeS<sub>2</sub> (on S), PbTe (on Te), PtAs<sub>2</sub> (on As), and the pure elements of Fe, Ni, Cu, Se, Ru, Rh, Pd, Ag, Sn, Sb, Pt, Au, and Bi.

The gradation was used to subdivide native gold as follows: very high-fineness 950‰–1000‰, high-fineness 900‰–950‰, medium-fineness 800‰–900‰, low-fineness 700‰–800‰, and electrum 300‰–700‰. The fineness of native gold was determined in permil (‰) by the formula  $Au/(Au+Ag+Hg) \times 1000$ ‰.

Fluid inclusions were analyzed using a TMS-600 Linkam stage equipped with LinkSystem 32 DV-NC (London, UK) and optical microscope Olympus BX51 (Olympus Corp., Tokyo, Japan). The first melting temperatures of fluid were interpreted using [15,16]. The salinity of fluids was identified from the final ice melting temperatures [17]. The homogenization temperatures of fluid inclusions are considered as the starting temperatures of the mineral formation process [18]. The gas phase composition of fluid inclusions was examined using a Horiba Jobin Yvon LabRam HR800 Raman spectrometer (Glasgow, Scotland) combined with a CCD detector and an Olympus BX51 microscope using a 532 nm Nd:YAG laser. The monochromator was calibrated to the silicon band (520.7 cm<sup>-1</sup>). Measurement data were processed in Statistica 6.1.

Pressure-temperature conditions for mineral assemblages were also determined using geothermometers (electrum-sphalerite paragenesis), geobarometers (electrum-sphalerite paragenesis), geofugometers, and mineral parageneses [19,20]. The stability areas of the main ore minerals in the  $fS_2 - fTe_2$  и  $fS_2 - fSe_2$  coordinates are examined from [21,22].

The isotopic composition of oxygen in quartz (samples BKO-4 and BKO-5, powder fraction 0.5–0.25 mm) was analyzed using laser fluorination in the Geospectr Analytical Center of the Geological Institute SB RAS (Ulan-Ude, Russia) on a FINNIGAN MAT 253 gas mass spectrometer using a double inflow system in the classical version (standard-sample) (analyst V.F. Posokhov).  $\delta^{18}O$  values are given in permil (‰) relative to the SMOW standard (NBS-28) [23]. The error of the obtained values did not exceed 0.2 to 0.3‰.

The sulfur isotopic composition in chalcopyrite (powder fractions 0.5–0.25 mm) was measured at the Multi-element and Isotope Research Center SB RAS using a Finnigan MAT Delta mass spectrometer in dual-inlet mode (analysts V.N. Reutsky and M.N. Kolbasova, Novosibirsk, Russia). The measurement control was provided by the samples with standard isotopic composition in the range  $\delta^{34}S$  from –15.1‰ to +21.8‰ relative to troilite from Canyon Diablo (CDT), including international ones: NBS-123 ( $\delta^{34}S = +17.44$ ) and NBS-127 ( $\delta^{34}S = +21.8$ ). The reproducibility of the values of  $\delta^{34}S$ , including sample preparation, was not more than 0.1‰ (2 $\sigma$ ). The values of  $\delta^{34}S$  (‰) are given relative to the CDT standard [23].

## 4. Results

### 4.1. Mineralogy

Hydrothermally altered quartz-sericite-kaolinite rocks with pyrite (up to 5%) occupied a large area in the ore occurrence, localizing within the tectonic fracture zone of SW trending. They are bleached, sericitized, silicified, and pyritized rocks with relic structures and formed predominantly in exocontacts of ore veins.

Early gold-sulfide-quartz veins (up to 1 m thick and 10 m long) are composed of quartz, pyrite, marcasite, pyrrhotite, arsenopyrite, chalcopyrite, and less frequently sphalerite, hessite, and gold. The ores have spotty, spotty-striped textures, and they have idiomorphic or panidiomorphic grained structures with superimposed cataclastic structures.

Quartz forms fine-grained aggregates and veins.

Pyrite is characterized by spotted clusters and chain-shaped phenocrysts consisting of large (1.7–2 to 5 mm) isometric polygonal grains or fine-grained aggregates with traces of cataclasis.

Marcasite and pyrite form spotted clusters elongated in discontinuous parallel-oriented bands.

Arsenopyrite (0.01–0.15 mm) forms hypidiomorphic grain chains and rare idiomorphic ingrowth in pyrite aggregates.

Sphalerite (up to 5 mm) is found in quartz, pyrite, and chalcopyrite as a phenocryst of xenomorphic grains (Figure 3).

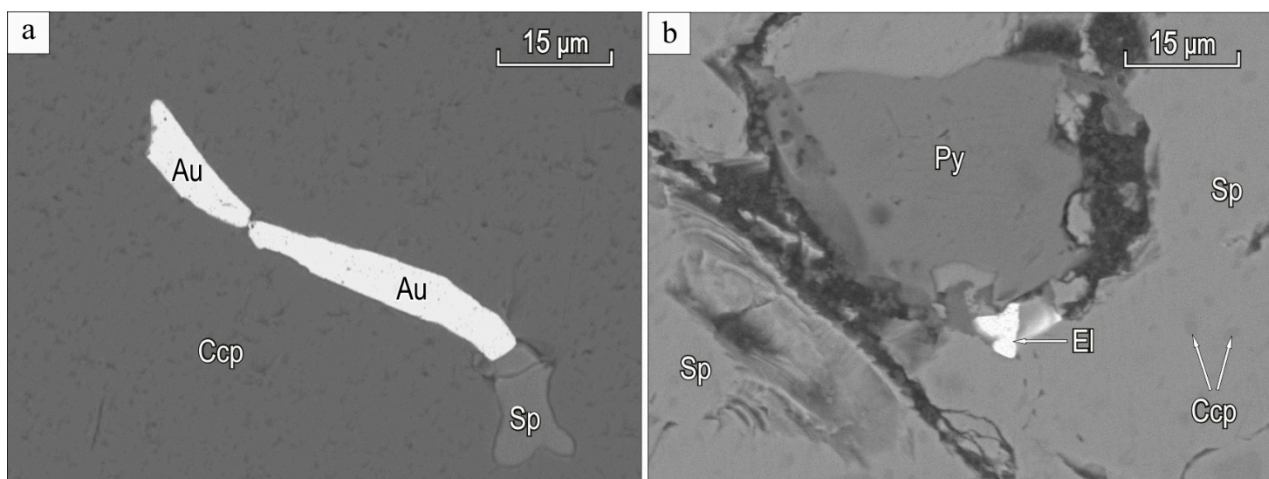


**Figure 3.** BSE-images of gold and electrum from gold-sulfide-quartz ore veins in Biche-Kadyr-Oos ore occurrence: (a) gold (Au) and sphalerite (Sp) in chalcopyrite (Ccp); (b) electrum (El) in the contact zone between pyrite (Py) and sphalerite (Sp).

Chalcopyrite (0.01 to 3 mm) often fills the finest cracks in quartz and forms emulsion phenocrysts in sphalerite (Figure 3b).

Hessite, tellurobismuthite, gold, and single grains of the electrum are observed as inclusions (up to 10 μm) in chalcopyrite and associated with sphalerite.

Gold and electrum are observed as thin inclusions in quartz and sulfides (Figure 3).

Native gold is categorized by Ag content (wt %):

- (1) Medium-fineness gold (Au 84.13–85.31, Ag 14.09–15.44);
- (2) low-fineness gold (Au 71.26–79.09, Ag 20.84–28.71);
- (3) electrum (Au 62.05–66.58, Ag 32.71–37.62).

The medium- and low-fineness gold and electrum (10.5%) dominate in gold-sulfide-quartz veins (Figure 4).

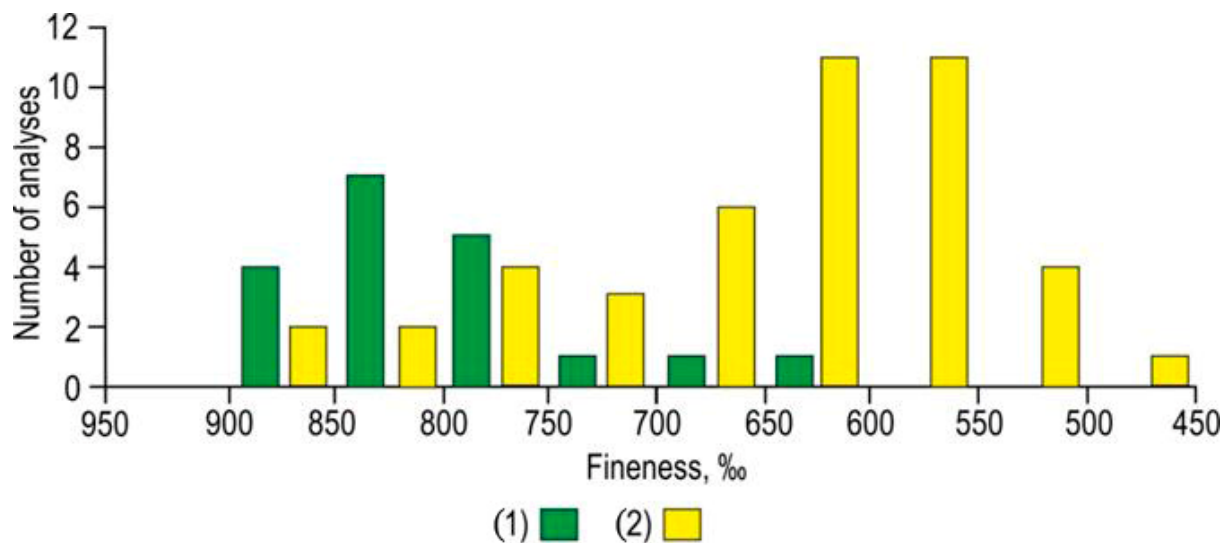


**Figure 4.** The native gold fineness distribution plot of gold-sulfide-quartz (1) and gold-polysulfide-carbonate-quartz (2) veins from Biche-Kadyr-Oos ore occurrence.

The late gold-polysulfide-carbonate-quartz veins (up to 1 m thick) and veined zones (up to 15 m) contain arsenopyrite, pyrite, chalcopyrite, sphalerite, and galena; less often, they contain fahlores, native Au, electrum, hessite ( $\text{Ag}_2\text{Te}$ ), tellurobismuthite ( $\text{Bi}_2\text{Te}_3$ ), bismuthinite ( $\text{Bi}_2\text{S}_3$ ), matildite ( $\text{AgBiS}_2$ ), jamesonite ( $\text{Pb}_4\text{FeSb}_6\text{S}_{14}$ ), and native Bi. Carbonates are represented by ankerite, siderite, and Fe-magnesite. The ores are characterized by massive, spotted, disseminated-veined, and disseminated-stained textures with elements of banded, disseminated, and veined textures. The main structures are cataclastic, breccia-like, and less frequently hypidiomorphic, subgraphic, and blastoporphyritic. Mineral aggregates developed in gold-polysulfide-carbonate-quartz veins develop along cracks and crushing zones of early pyrite of the gold-sulfide-quartz stage (Figure 5a).

Arsenopyrite (up to 2.5 mm), pyrite (up to 1.5 mm), and sphalerite (up to 5 mm) formed isolated aggregates of isometric or elongated shape in quartz or chalcopyrite. Some sphalerite grains are characterized by Fe admixture up to 15 wt %. Chalcopyrite and bornite (up to 5 mm) are present as granular precipitates in quartz. Fahlores of the tennantite–tetrahedrite series were found in intergrowths with chalcopyrite.

Galena formed isolated aggregates (up to 0.8 mm) and finest phenocrysts in chalcopyrite, pyrite, and carbonate. The boundaries of galena grains are uneven, rectilinear, and stepped (see Figure 5). Galena contains impurities of Ag up to 1.85 wt % and Se up to 5 wt %. Ni-cobaltite and Co-gersdorffite are located at the boundaries of pyrite and chalcopyrite grains and form inclusions in chalcopyrite.

Bismuthite (up to 10  $\mu\text{m}$ ), tellurobismuthite (up to 5  $\mu\text{m}$ ), and matildite (up to 15  $\mu\text{m}$ ) are found as inclusions in chalcopyrite and pyrite and are associated with arsenopyrite, native Au, and electrum (see Figure 5).

Se-acanthite (up to 5  $\mu\text{m}$ ) with arsenopyrite formed inclusions in chalcopyrite (see Figure 5).

Inclusions of matildite and ourayite up to 15  $\mu\text{m}$  in size were found in pyrite.

Native Bi (up to 5  $\mu\text{m}$ ) formed thin “fines” in quartz.

Small inclusions of hessite (up to 10  $\mu\text{m}$ ) of rounded, oval, and twisted shapes were observed in the chalcopyrite associated with gold and the electrum.

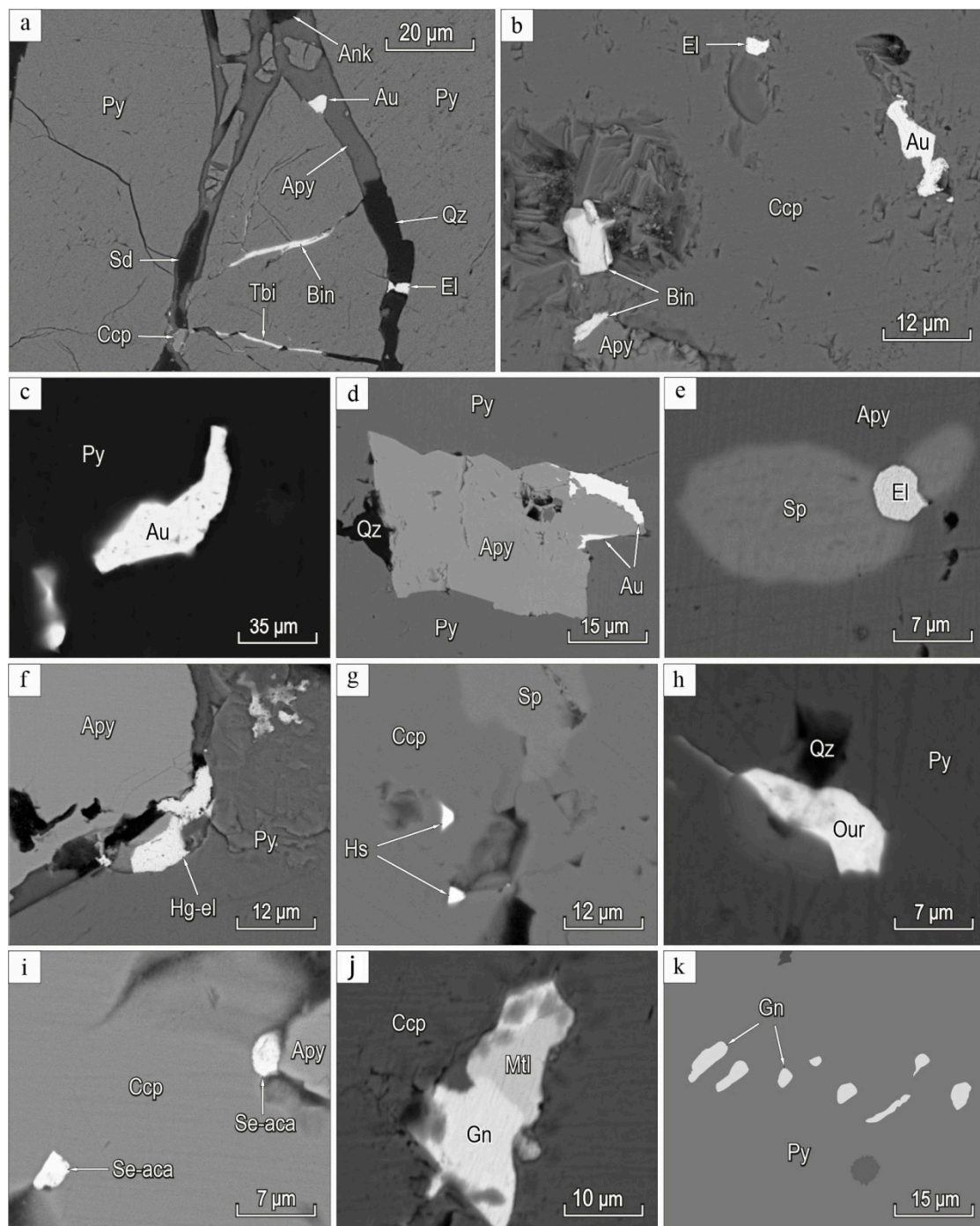


**Figure 5.** BSE-images of the minerals of gold-polysulfide-carbonate-quartz ore veins in Biche-Kadyr-Oos ore occurrence: (a) gold (Au), electrum (El), tellurobismuthite (Tbi), bismuthinite (Bin), ankerite (Ank), siderite (Sd), and chalcopyrite (Ccp) develop along cracks and crushing zones, cementing pyrite (Py) grains in gold-sulfide-quartz stages; (b) gold inclusions (Au), electrum (El), bismuthinite (Bin), and arsenopyrite (Apy) in chalcopyrite (Ccp); (c) gold (Au) in quartz; (d) intergrowths of gold (Au), and arsenopyrite (Apy) in pyrite (Py); (e) inclusions of electrum (El), and sphalerite (Sp) in arsenopyrite (Apy); (f) Hg-electrum (Hg-el) with arsenopyrite (Apy) and pyrite (Py); (g) inclusions of hessite (Hs) and sphalerite (Sp) in quartz; (h) quartz (Qz) and ourayite (Our) in pyrite (Py); (i) Se-acanthite (Se-aca) inclusions in chalcopyrite (Ccp) with arsenopyrite (Apy); (j) matildite (Mtl) and galena (Gn) in chalcopyrite (Ccp); (k) galena (Gn) inclusion in pyrite (Py).

The compositions of Bi and Te minerals are shown in Table 1.

**Table 1.** The chemical composition of hessite, Se-acanthite, matildite, ourayite, bismuthine, and Te-bismuthite from Biche-Kadyr-Oos ore occurrence (wt %).

Point No	Ag	Bi	Te	Pb	S	Se	Sum	Crystal Chemical Formula
Hessite								
1	62.78	–	37.12	–	–	–	99.90	Ag <sub>2.00</sub> Te <sub>1.00</sub>
2	62.85	–	36.76	–	–	–	99.61	Ag <sub>2.01</sub> Te <sub>0.99</sub>
3	63.70	–	36.21	–	–	–	99.91	Ag <sub>2.03</sub> Te <sub>0.97</sub>
4	62.87	–	36.25	–	–	–	99.12	Ag <sub>2.02</sub> Te <sub>0.98</sub>
5	62.71	–	36.78	–	–	–	99.49	Ag <sub>2.01</sub> Te <sub>0.99</sub>
6	62.69	–	37.27	–	–	–	99.96	Ag <sub>2.00</sub> Te <sub>1.00</sub>
7	62.88	–	36.25	–	–	–	99.13	Ag <sub>1.98</sub> Te <sub>1.02</sub>
Se-acanthite								
8	80.94	–	–	–	7.51	11.24	99.69	Ag <sub>2.00</sub> (S <sub>0.62</sub> Se <sub>0.38</sub> ) <sub>1.00</sub>
Matildite								
9	27.37	55.89	–	–	16.66	–	99.92	Ag <sub>0.98</sub> Bi <sub>1.02</sub> S <sub>2.00</sub>
Ourayite								
10	12.11	42.87	–	27.91	16.12	–	99.01	Ag <sub>2.94</sub> Pb <sub>3.53</sub> Bi <sub>5.37</sub> S <sub>13.16</sub>
Tellurobismuthite								
11	–	52.42	46.85	–	–	–	99.27	Bi <sub>2.03</sub> Te <sub>2.97</sub>
Bismuthinite								
12	–	80.67	–	–	18.63	–	99.30	Bi <sub>2.00</sub> S <sub>3.00</sub>
13	–	81.04	–	–	18.62	–	99.66	Bi <sub>2.00</sub> S <sub>3.00</sub>
14	–	80.78	–	–	18.74	–	99.52	Bi <sub>1.99</sub> S <sub>3.01</sub>
15	–	81.25	–	–	18.62	–	99.87	Bi <sub>2.01</sub> S <sub>2.99</sub>

*Note.* A dash indicates the value was below detection limits. The formulas of hessite are calculated for 2 at., Se-acanthite for 3 at., matildite for 4 at., tellurobismuthite and bismuthinite for 5 at.

Native gold and electrum in gold-polysulfide-carbonate-quartz veins are composed of grains from 3 µm to 1.5 mm in chalcopyrite, pyrite, and arsenopyrite. The predominant forms are fracture-vein, lumpy-branchy, lumpy-cellular, dendritic, and interstitial. Native Au and electrum form intergrowths with chalcopyrite, arsenopyrite, galena, tellurobismuthite, bismuthinite, Se-acanthite, and barite (Figure 5).

Native gold by Ag and Hg content is subdivided (wt %):

- (1) medium-fineness gold (Au 82.92–86.94, Ag 13.51–17.04);
- (2) low-fineness gold (Au 69.76–79.44, Ag 19.81–29.93);
- (3) electrum (Au 51.82–69.15, Ag 30.83–48.13);
- (4) Hg-electrum (Au 49.48–56.99, Ag 37.30–43.11, Hg 5.03–6.52).

The Ag value in gold is up to 29.93 wt %; in electrum—48.13 wt %, Hg—6.52 wt % (Table 2). A single grain of Hg-electrum (20 µm) was found at the contact of pyrite with brecciated arsenopyrite. The gold-polysulfide-carbonate-quartz veins are quantitatively dominated by electrum and low-fineness and medium-fineness gold (Figure 4).

**Table 2.** Chemical composition of zoned gold from Biche-Kadyr-Oos ore occurrence, wt %.

Analysis No.	Zone	Au	Ag	Hg	Sum	Crystallochemical Formula	Fineness
1-1	Core	86.49	13.51	–	100	(Au <sub>0.78</sub> Ag <sub>0.22</sub> ) <sub>1.00</sub>	865
1-2	Edge	52.85	47.11	–	99.96	(Ag <sub>0.62</sub> Au <sub>0.88</sub> ) <sub>1.00</sub>	528
2-1	Core	86.46	13.51	–	99.97	(Au <sub>0.78</sub> Ag <sub>0.22</sub> ) <sub>1.00</sub>	865
2-2	Edge	56.91	43.07	–	99.91	(Ag <sub>0.58</sub> Au <sub>0.42</sub> ) <sub>1.00</sub>	569
3-1	Core	85.31	14.09	–	99.40	(Au <sub>0.77</sub> Ag <sub>0.23</sub> ) <sub>1.00</sub>	858
3-2	Edge	66.58	32.71	–	99.29	(Au <sub>0.53</sub> Ag <sub>0.47</sub> ) <sub>1.00</sub>	671
4-1	Core	85.13	14.45	–	99.58	(Au <sub>0.76</sub> Ag <sub>0.24</sub> ) <sub>1.00</sub>	855
4-2	Edge	84.25	15.44	–	99.69	(Au <sub>0.75</sub> Ag <sub>0.25</sub> ) <sub>1.00</sub>	845
5-1	Core	85.41	13.95	–	99.36	(Au <sub>0.77</sub> Ag <sub>0.23</sub> ) <sub>1.00</sub>	860
5-2	Edge	69.76	29.93	–	99.69	(Au <sub>0.56</sub> Ag <sub>0.44</sub> ) <sub>1.00</sub>	700
5-3	Edge	61.55	38.44	–	99.99	(Au <sub>0.47</sub> Ag <sub>0.53</sub> ) <sub>1.00</sub>	616
6-1	Core	82.96	17.04	–	100	(Au <sub>0.73</sub> Ag <sub>0.27</sub> ) <sub>1.00</sub>	830
6-2	Edge	69.76	29.93	–	99.69	(Au <sub>0.56</sub> Ag <sub>0.44</sub> ) <sub>1.00</sub>	700
7-1	Core	79.08	20.84	–	99.92	(Au <sub>0.68</sub> Ag <sub>0.32</sub> ) <sub>1.00</sub>	791
7-2	Edge	70.42	29.15	–	99.57	(Au <sub>0.57</sub> Ag <sub>0.43</sub> ) <sub>1.00</sub>	707
8-1	Core	71.98	28.01	–	99.99	(Au <sub>0.58</sub> Ag <sub>0.42</sub> ) <sub>1.00</sub>	720
8-2	Edge	60.22	39.75	–	99.97	(Au <sub>0.45</sub> Ag <sub>0.56</sub> ) <sub>1.00</sub>	602
9-1	Core	75.68	23.96	–	99.64	(Au <sub>0.63</sub> Ag <sub>0.37</sub> ) <sub>1.00</sub>	760
9-2	Edge	71.26	28.71	–	99.97	(Au <sub>0.58</sub> Ag <sub>0.42</sub> ) <sub>1.00</sub>	713
10-1	Core	69.15	30.83	–	99.98	(Au <sub>0.55</sub> Ag <sub>0.45</sub> ) <sub>1.00</sub>	692
10-2	Edge	55.62	45.25	–	100.87	(Au <sub>0.40</sub> Ag <sub>0.60</sub> ) <sub>1.00</sub>	551
11-1	Core	68.25	31.06	–	99.31	(Au <sub>0.55</sub> Ag <sub>0.45</sub> ) <sub>1.00</sub>	687
11-2	Edge	55.01	44.97	–	99.98	(Au <sub>0.40</sub> Ag <sub>0.60</sub> ) <sub>1.00</sub>	550
12-1	Core	68.22	31.39	–	99.64	(Au <sub>0.54</sub> Ag <sub>0.46</sub> ) <sub>1.00</sub>	685
12-2	Edge	60.22	39.75	–	99.97	(Ag <sub>0.55</sub> Au <sub>0.45</sub> ) <sub>1.00</sub>	602
13-1	Core	66.51	33.14	–	99.65	(Au <sub>0.52</sub> Ag <sub>0.48</sub> ) <sub>1.00</sub>	667
13-2	Edge	62.53	37.04	–	99.57	(Au <sub>0.48</sub> Ag <sub>0.52</sub> ) <sub>1.00</sub>	628
14-1	Core	60.43	39.19	–	99.62	(Au <sub>0.46</sub> Ag <sub>0.54</sub> ) <sub>1.00</sub>	607
14-2	Edge	51.90	48.07	–	99.97	(Au <sub>0.37</sub> Ag <sub>0.63</sub> ) <sub>1.00</sub>	519
15-1	Core	59.04	40.43	–	99.47	(Au <sub>0.44</sub> Ag <sub>0.56</sub> ) <sub>1.00</sub>	594
15-2	Edge	58.44	41.53	–	99.97	(Au <sub>0.44</sub> Ag <sub>0.56</sub> ) <sub>1.00</sub>	585
16-1	Core	56.99	37.30	5.03	99.32	(Ag <sub>0.52</sub> Au <sub>0.43</sub> Hg <sub>0.04</sub> ) <sub>1.00</sub>	574
16-2	Edge	49.48	43.11	6.52	99.11	(Ag <sub>0.58</sub> Au <sub>0.37</sub> Hg <sub>0.05</sub> ) <sub>1.00</sub>	499
17-1	Core	56.81	43.09	–	99.90	(Au <sub>0.42</sub> Ag <sub>0.58</sub> ) <sub>1.00</sub>	569
17-2	Edge	56.14	43.81	–	99.95	(Au <sub>0.41</sub> Ag <sub>0.59</sub> ) <sub>1.00</sub>	562
18-1	Core	52.85	47.11	–	99.96	(Au <sub>0.40</sub> Ag <sub>0.60</sub> ) <sub>1.00</sub>	529
18-2	Edge	51.82	48.13	–	99.95	(Au <sub>0.37</sub> Ag <sub>0.63</sub> ) <sub>1.00</sub>	518

*Note.* The table shows the most representative analyzes of native gold grains. A dash indicates the value was below detection limits. The Au chemical composition was examined on SEM equipped with MIRA LM EDS (operator N.S. Karmanov, IGM SB RAS, Novosibirsk, Russia). The chemical composition of gold was calculated using the sum of metals equal to 1. The fineness of native gold was determined in permil (‰) by the formula  $Au/(Au + Ag + Hg) \times 1000\%$ .

The main impurities in gold are Ag and Hg, and the Cu content is below the detection limit. The average fineness of gold of the ore occurrence is 687 with variations from 865 to 499, while the average fineness gold-sulfide-quartz veins is 791 (622–858); for gold-polysulfide-carbonate-quartz veins is 663 (499–865‰). In general, the ores are quantitatively dominated by electrum and medium-fineness and low-fineness gold (see Figure 4).

Based on [1] and our observations, we divided the Biche-Kadyr-Oos ore occurrence into three stages: (1) argillic; (2) gold-sulfide-quartz; and (3) gold-polysulfide-carbonate-quartz (Figure 6).

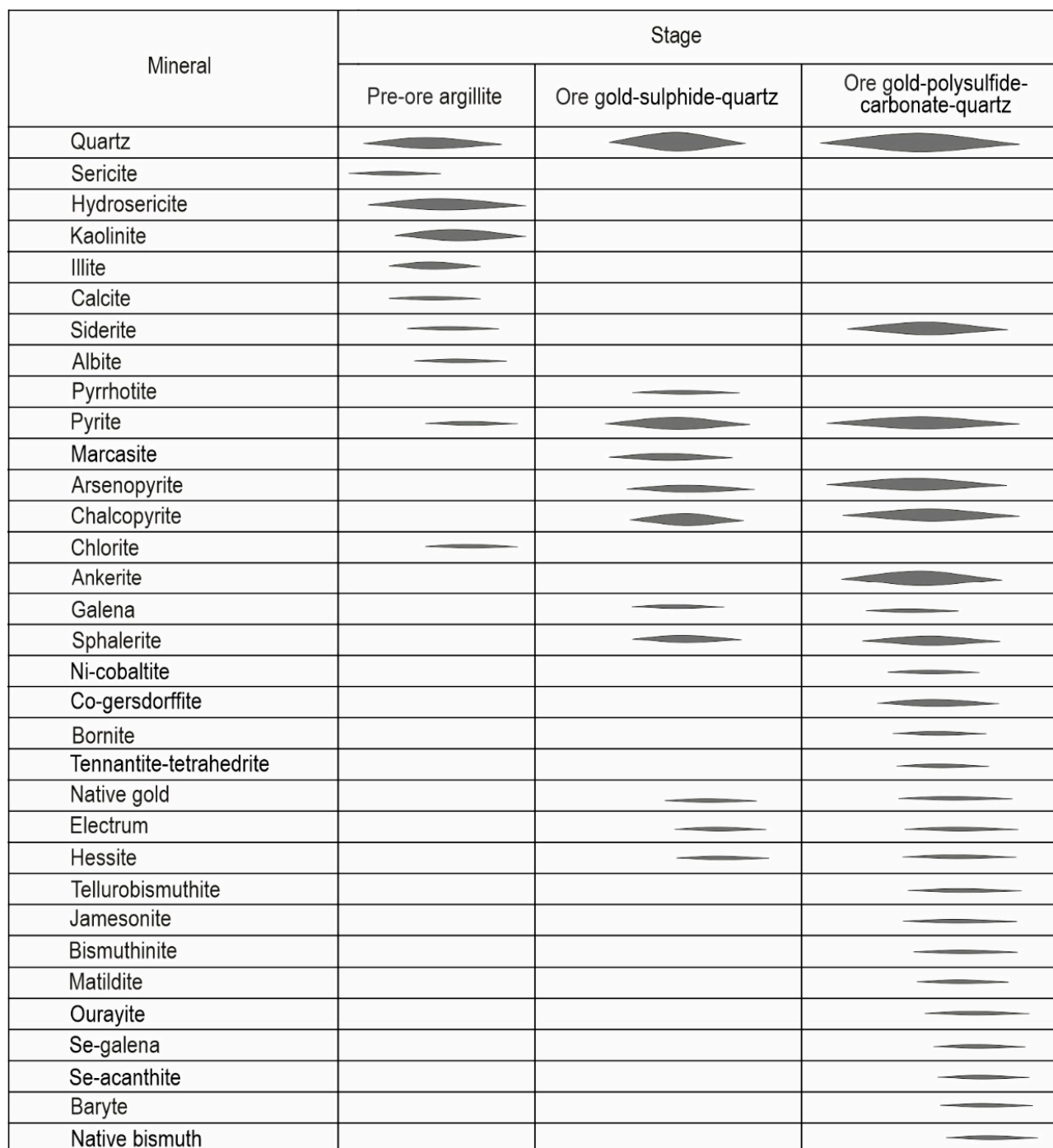


**Figure 6.** The paragenetic sequence of Biche-Kadyr-Oos ore occurrence. The line thickness indicates the relative mineral prevalence.

#### 4.2. Conditions for the Formation of Ore Mineral Veins

Fluid inclusions were studied in quartz of ore veins to determine the PT conditions of mineral-forming fluid in the Biche-Kadyr-Oos ore occurrence.

We analyzed two-phased (VL) primary and pseudosecondary fluid inclusions in quartz, which are located in the central parts of grains and unrelated to fractures. They are 12–15  $\mu\text{m}$  size (rarely up to 20  $\mu\text{m}$ ), round-oval or isometric in shape, sometimes with crystallographic elements. Vapor bubbles occupied up to 15%–20% of the inclusions (Figure 7).

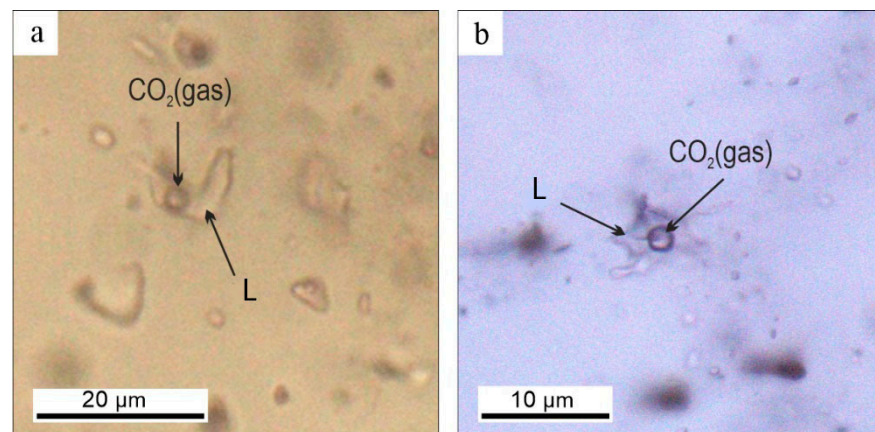


**Figure 7.** Fluid inclusions in quartz in gold-sulfide-quartz (a), and gold-polysulfide-carbonate-quartz (b) veins of the Biche-Kadyr-Oos ore occurrence. L—liquid.

The fluid inclusions in quartz of gold-sulfide-quartz veins contain Na-K-chloride fluid with first melting temperatures (from  $-23$  to  $-24$  °C) (Table 3). Fluid inclusions were homogenized at  $250$ – $292$  °C; the fluid salinity varies from  $4.9$  to  $8.6$  wt % NaCl eqv.

**Table 3.** Fluid inclusion data of quartz from Biche-Kadyr-Oos ore occurrence.

Sample	Phase Composition	n	$T_{\text{hom}}$ , °C	$T_{\text{eut}}$ , °C	$T_{\text{melt.ice}}$ , (°C)	Salinity, (wt % NaCl eqv)	Fluid Composition
Gold-sulfide-quartz veins							
BKO-4	VL	46	290–230	$-23 \dots -24$	$-3 \dots -5.6$	4.9–8.6	NaCl-KCl-H <sub>2</sub> O + CO <sub>2</sub>
Gold-polysulfide-carbonate-quartz veins							
BKO-3	VL	55	225–255	$-23$	$-4 \dots -5.3$	6–8.2	NaCl-KCl-H <sub>2</sub> O + CO <sub>2</sub>
BKO-5	VL	50	230–253	$-21 \dots -22$	$-3 \dots -6.1$	4.9–9.5	NaCl-H <sub>2</sub> O

Note. VL—biphase (vapour+liquid). n—the number of analyzes.  $T_{\text{hom}}$ —homogenization temperatures,  $T_{\text{eut}}$ —eutectic (first melting) temperatures;  $T_{\text{melt.ice}}$ —final melting temperatures.

The fluid inclusions in quartz of gold-polysulfide-carbonate-quartz veins were homogenized at lower temperatures of  $225$ – $258$  °C. The fluid salinity increases up to  $8.2$ – $9.3$  wt % NaCl equiv. Raman spectroscopy data indicate that the gas phase consists of CO<sub>2</sub>.

Due to the data of the composition of native Au (atomic amount of Ag in native gold) and ferruginicity ( $X_{\text{FeS}}$ ) of sphalerite coexisting with native gold, we estimated the temperatures of gold-sulfide-quartz ( $300$ – $287$  °C, average  $295$  °C) and gold-polysulfide-carbonate-quartz ( $290$ – $200$  °C, average  $275$  °C) veins formation using an electrom-sphalerite geothermometer [19]. Temperatures were calculated by the following formula:  $T^{\circ}\text{K} = \{28,765 + 22,600(1 - N_{\text{Ag}})^2 - 6400(1 - N_{\text{Ag}})^3\} / \{49.008 - 9.152 \log X_{\text{FeS}} + 18.2961 \log N_{\text{Ag}} + 5.5(1 - N_{\text{Ag}})^2\}$ .

Paragenesis of pyrite, pyrrhotite, chalcopyrite, and arsenopyrite of early gold-sulfide-quartz veins indicates that  $fS_2$  ranged from  $10$ – $14.3$  to  $10$ – $7.6$  at  $300$  °C; the paragenesis of native Bi, matildite, Se-acanthite, and other sulfides of the late gold-polysulfide-carbonate-quartz veins indicates the redox potential changes in the fluid at variations of  $fS_2$  ranged from  $10^{-17.8}$  to  $10^{-10.7}$ ,  $fTe_2$  from  $10^{-17}$  to  $10^{-11.4}$ , and  $fSe_2$  from  $10^{-21}$ – $10^{-12}$  at  $200$  °C [19,20].

The pressure during the formation of the late quartz veins was calculated using a sphalerite geobarometer [20]. According to the electrom-sphalerite geothermometer, the pressure during the vein formation was estimated at  $0.5$  kbar at sphalerite crystallization temperatures equal to  $275$  °C.

#### 4.3. Ore Fluid Isotopic Composition of S and O

The isotopic composition of sulfur in chalcopyrite from early gold-sulfide-quartz veins varies from +4.8‰ to +5.4‰; and sulfides from the latest gold-polysulfide-carbonate-quartz veins vary from +3.0 to +4.9 (pyrite ranges from +3.0‰ to +3.3‰, chalcopyrite—+4.9‰). According to the fractionation equation [24,25] and mineral formation temperatures according to the electrum-sphalerite geothermometer [19], the  $\delta^{34}\text{S}_{\text{H}_2\text{S}}$  values of the fluid for early ore veins vary from +4.2‰ to +4.7‰ ( $T = 295\text{ }^\circ\text{C}$ ), and, for late ore veins, from +1.3‰ to +4.9‰ ( $T = 275\text{ }^\circ\text{C}$ ), indicating the involvement of magmatic sulfur and magmatic fluid genesis [24–27].

The  $\delta^{18}\text{O}$  value of quartz from early ore veins varies from 11.8 to 13.8‰. According to the fractionation equation [28,29],  $\delta^{18}\text{O}$  values of the fluid of the gold-sulfide-quartz veins (sample BKO-4) are +6.4‰ ( $T = 295\text{ }^\circ\text{C}$ ) and those of the gold-polysulfide-carbonate-quartz veins (sample BKO-5) are +3.5‰ ( $T = 275\text{ }^\circ\text{C}$ ). The  $\delta^{34}\text{S}_{\text{H}_2\text{S}}$  (+1.4‰ to +5.3‰) and  $\delta^{18}\text{O}_{\text{H}_2\text{O}}$  (from +3.4‰ to +6.5‰) values of the fluid suggest that magmatic fluids mixed with meteoric water ( $\delta^{18}\text{O}_{\text{H}_2\text{O}}$  see Figure 8).

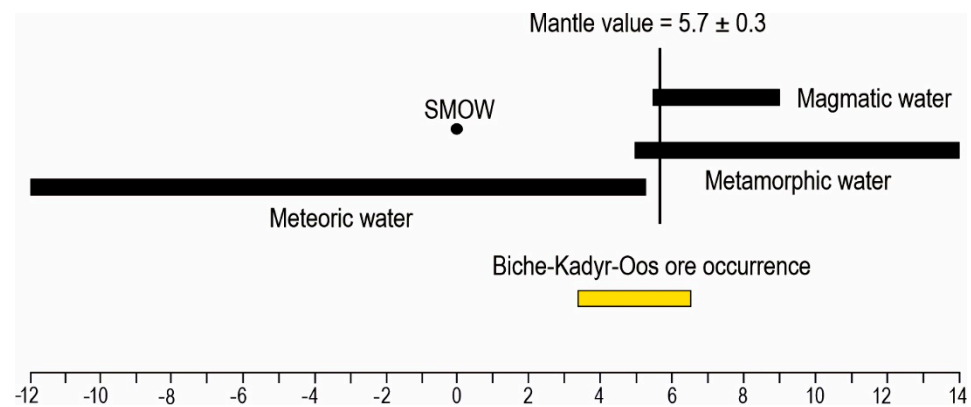


**Figure 8.** Oxygen isotopic composition of fluid from Biche-Kadyr-Oos ore occurrence. Oxygen isotope compositions of metamorphic, meteoric, and magmatic water, after Rollinson [30].

## 5. Discussion

Ore mineralization is associated with quartz-sericite-kaolinite and quartz-sericite-kaolinite-illilitic alteration of host volcano-sedimentary rocks, and granite-porphyry intrusion of the Ak-Sug complex (C<sub>1</sub>ak).

Hydrothermal alteration of rocks is close to mineralized areas and confined to zones of induced fracturing.

The mineral composition of the early gold-sulfide-quartz veins consists of simple sulfides, gold, electrum, and single hessite segregations.

Gold-polysulfide-carbonate-quartz veins contain gold, electrum, Hg-electrum, Se-acanthite, Se-galena, hessite, tellurobismuthite, bismuthinite, matildite, and other minerals typical for epithermal Au-Ag deposits [31–35]. A similar mineral composition was determined for the late stages of the Ak-Sug Cu-Au-Mo porphyry deposit in argillic [36].

With the pressure correction (0.5 kbar) [37], the fluid inclusion data showed that gold-sulfide-quartz veins were formed at temperatures ranging from 330 to 270 °C due to Na-K chloride fluid with a salinity of 4.9 to 8.6 wt % NaCl eqv.

The late gold-polysulfide-carbonate-quartz veins were formed at temperatures ranging from 290 to 260 °C due to Na-K chloride fluid with salinities from 4.9 to 9.6 wt % NaCl equiv. These data are consistent with mineral geothermometers. Paragenesis of pyrite, pyrrhotite, chalcopyrite, and arsenopyrite from gold-sulfide-quartz veins suggests  $f\text{S}_2$  from  $10^{-14.3}$  to  $10^{-7.6}$  at 295 °C.

Paragenesis of native Bi, matildite, Se-acanthite, and other sulfides of gold-polysulfide-carbonate-quartz veins indicates the redox potential changes of the fluid at variations

of  $fS_2$  from  $10^{-17.8}$  to  $10^{-10.7}$ ,  $fTe_2$  from  $10^{-17}$  to  $10^{-11.4}$ , and  $fSe_2$  from  $10^{-21}$ – $10^{-12}$  at 200 °C [21,22].

The  $\delta^{34}S_{H_2S}$  and  $\delta^{18}O_{H_2O}$  values indicate the magmatic fluid mixed with meteoric water. We suggest that the magmatic fluid was separated from the deep intrusions of the Ak-Sug complex (Є<sub>1ak</sub>). The meteoric water participation is typical for epithermal Au-Ag deposits [38–40] and for late stages of gold-copper-porphyry deposits [41–46].

According to Sillitoe [8], gold mineralization is located both directly in the ore stockwork of porphyry Cu mineralization and outside. A classic example is the Bingham deposit, where a Cu porphyry stockwork is surrounded by copper-gold skarns and, in turn, copper-zinc and gold-silver mineralization is confined to its periphery [8]. In the second way, it is located in HS and IS epithermal mineralization, sub-epithermal (transitional from post-porphyry to epithermal) carbonate-polymetallic ores and accompanied by Ag minerals [47]. In other cases, epithermal mineralization is formed at a distance from Cu-porphyry deposits (up to several kilometers): as Lepanto relative to the Far South East deposit, Philippines.

Mineralogical and geochemical peculiarities and formation of Biche-Kadyr-Oos ores from fluids of mixed meteoric vs. magmatic origin and confinement of gold mineralization to sulfide-quartz and polysulfide-quartz veins with argillite zones indicate that the ore occurrence can be attributed to epithermal intermediate sulfidation (IS) type [9,48]. We noted that the indicator minerals of IS type mineralization are sphalerite, galena, tetrahedrite-tennantite, chalcopyrite, and manganese carbonates. Examples of deposits with IS-type mineralization are Santa Barbara (Greece) [49] and Mount Milligan (Canada) [47].

The epithermal Au-Ag mineralization of IS type, as well as Zn-Pb-Ag ± Cu ± Au veined IS type deposits, localized near copper-porphyry deposits are associated with porphyry-epithermal systems with argillites [8].

## 6. Conclusions

Thus, according to the mineralogical and geochemical features and formation conditions, the Biche-Kadyr-Oos ore occurrence can be categorized as an epithermal Au-Ag deposit of intermediate sulfidation type. When searching for porphyry Cu mineralization, detecting different types of accompanying ores gives us other important information. Epithermal Au-Ag mineralization on the Biche-Kadyr-Oos ore occurrence is similar to the final stages of mineralization of gold-copper-porphyry deposit Ak-Sug, developed at the Biche-Kadyr-Oos ore occurrence and located 12 km to the NW, but developed at a distance as sulfide-quartz and polysulfide-carbonate-quartz veins in quartz-sericite-caolinite argillic of the Lower Cambrian effusive-sedimentary rocks. The type of mineralization indicates the degree of preservation of porphyry-epithermal systems and the level of the erosion cut-off. The obtained results may be of practical importance for regional predictive-metallogenic prospecting of Cu, Ag, and Au deposits and ore occurrences.

**Author Contributions:** Conceptualization, R.V.K.; methodology R.V.K. and N.N.A.; expeditionary work R.V.K., A.K.H., Y.V.B. and S.N.S.; investigation R.V.K., N.N.A. and N.V.S.-M.; visualization R.V.K. and N.V.S.-M.; writing—original draft preparation R.V.K. and N.N.A.; review and editing R.V.K., B.B.D., Y.A.K. and F.P.; writing—review and editing R.V.K., N.N.A. and F.P.; project administration, R.V.K. All authors have read and agreed to the published version of the manuscript.

**Funding:** This research was funded by the Russian Science Foundation (grant no. 23-27-00344).

**Data Availability Statement:** Data are contained within the article.

**Acknowledgments:** The authors are deeply grateful to the reviewers for allowing us to make this paper better.

**Conflicts of Interest:** The authors declare no conflict of interest.

## References

1. Stamborovskiy, N.N.; Smolyakov, Y.G. *Geologicheskoe Stroenie i Poleznye Iskopaemye Bassejna Verhnih Techenij Rek Ak-Suga, Soruga i Kadyr-Osca*; Kyzyl, Russia, 1969; p. 356. (In Russian)
2. Zabelin, V.I. *Geologicheskoe Stroenie i Geologo-Geohimicheskaya Zonalnost' Ak-Sugskogo Medno-Porfirovogo Mestorozhdeniya Kak Kriterij Glubinnogo Prognozirovaniya*; Diss. kand. geol.-min. nauk.: Kyzyl, Russia, 1988; 145p. (In Russian)
3. Berzina, A.N.; Berzina, A.P.; Gimon, V.O. Paleozoic-Mesozoic Porphyry Cu(Mo) and Mo(Cu) Deposits within the Southern Margin of the Siberian Craton: Geochemistry, Geochronology, and Petrogenesis (a Review). *Minerals* **2016**, *6*, 125. [[CrossRef](#)]
4. Berzina, A.N.; Stein, H.J.; Zimmerman, A.; Sotnikov, V.I. Re-Os ages of molybdenite from porphyry and greisen Mo-W deposits of southern Siberia (Russia) preserve metallogenic record. In *Mineral Exploration and Sustainable Development*; Eliopoulos, D., Ed.; Millpress: Rotterdam, Netherlands, 2003; pp. 231–234.
5. Pollard, P.J.; Pelenkova, E.; Mathur, R. Paragenesis and Re-Os molybdenite age of the Cambrian Ak-Sug porphyry Cu-Au-Mo deposit, Tyva Republic, Russian Federation. *Econ. Geol.* **2017**, *112*, 1021–1028. [[CrossRef](#)]
6. Gusev, N.I.; Berzon, E.I.; Semenov, M.I. Kyzyk–Chadr porphyry copper deposit (Tuva): Geochemical features and age constraints on magmatism. *Reg. Geol. Metallog.* **2014**, *59*, 70–79. (In Russian)
7. Sillitoe, R.H. *Exploration of Porphyry Copper Lithocaps/Pacific Rim Congress*; The Australasian Institute of Mining and Metallurgy: Melbourne, Australia, 1995; pp. 527–532.
8. Sillitoe, R.H. Porphyry Copper Systems. *Econ. Geol.* **2010**, *105*, 3–41. [[CrossRef](#)]
9. White, N.C.; Hedenquist, J.W. Epithermal gold deposits: Styles, characteristics, and exploration. *Soc. Econ. Geol. Newsl.* **1995**, *23*, 9–13. [[CrossRef](#)]
10. Berzin, N.A.; Coleman, R.G.; Dobretsov, N.L.; Zonenshain, L.P.; Xiao, X.; Chang, E.Z. Geodynamic map of the western part of Paleasian Ocean. *Russ. Geol. Geophys.* **1994**, *35*, 5–22.
11. Berzin, N.A.; Kungurtsev, L.V. Geodynamic interpretation of Altai–Sayan Geological complexes. *Russ. Geol. Geophys.* **1996**, *37*, 56–73.
12. Yarmolyuk, V.V.; Kovalenko, V.I. Batholiths and geodynamics of batholiths formation in the Central Asian Fold Belt. *Russ. Geol. Geophys.* **2003**, *44*, 1260–1274.
13. Rudnev, S.N.; Serov, P.A.; Kiseleva, V.Y. Vendian-Early Paleozoic granitoid magmatism in Eastern Tuva. *Russ. Geol. Geophys.* **2015**, *56*, 1232–1255. [[CrossRef](#)]
14. Mongush, A.A. Geological position, geochemical and Sm-Nd-isotopic composition of ophiolites of the Sayan-Tuva forearc zone. *Bull. Tomsk. Polytech. Univ. Geo Assets Eng.* **2019**, *30*, 56–75. [[CrossRef](#)]
15. Borisenko, A.S. Study of the salt composition of solutions of gas–liquid inclusions in minerals by the cryometric method. *Russ. Geol. Geophys.* **1977**, *18*, 16–27.
16. Davis, D.W.; Lowenstein, T.K.; Spenser, R.J. Melting behavior of fluid inclusions in laboratory-grown halite crystals in the systems NaCl–H<sub>2</sub>O, NaCl–KCl–H<sub>2</sub>O, NaCl–MgCl<sub>2</sub>–H<sub>2</sub>O, and CaCl<sub>2</sub>–NaCl–H<sub>2</sub>O. *Geochim. Cosmochim. Acta.* **1990**, *54*, 591–601. [[CrossRef](#)]
17. Bodnar, R.J.; Vityk, M.O. Interpretation of microthermometric data for H<sub>2</sub>O–NaCl fluid inclusions. In *Fluid Inclusions in Minerals: Methods and Applications*; De Vivo, B., Frezzotti, M.L., Eds.; Fluids Research Laboratory, Department of Geological Sciences, Virginia Tech: Blacksburg, VA, USA, 1994; pp. 117–130.
18. Roedder, E. Fluid inclusions. In *Reviews in Mineralogy and Geochemistry*; De Gruyter: Berlin, Germany, 1984; Volume 12, p. 646.
19. Barton, P.B.; Skinner, B.J. Sulfide mineral stabilities. In *Geochemistry of Hydrothermal Ore Deposits*; Barnes, H.L., Ed.; Siley & Sons: New York, NY, USA, 1979; pp. 278–403.
20. Afifi, A.M.; Kelly, W.C.; Essene, E.J. Phase relations among tellurides, sulphides and oxides: I. Thermochemical data and calculated equilibria. *Econ. Geol.* **1988**, *83*, 377–404. [[CrossRef](#)]
21. Shikazono, N. A comparison of temperatures estimated from the electrum-sphalerite-pyrite-argentite assemblage and filling temperatures of fluid implications from epithermal Au-Ag vein-type deposits in Japan. *Econ. Geol.* **1985**, *80*, 1415–1424. [[CrossRef](#)]
22. Toulmin, P.; Barton, P.B.; Wiggins, L.B. Commentary on the sphalerite geobarometer. *Am. Mineral.* **1991**, *76*, 1038–1051.
23. Coplen, T.B. Normalization of oxygen and hydrogen data. *Chem. Geol.* **1988**, *72*, 293–297.
24. Ohmoto, H.; Rye, R.O. Isotopes of Sulfur and Carbon. In *Geochemistry of Hydrothermal Ore Deposits*; Wiley: New York, NY, USA, 1979; pp. 509–567.
25. Li, Y.; Liu, J. Calculation of sulfur isotope fractionation in sulfides. *Geochim. Cosmochim. Acta* **2006**, *70*, 1789–1795. [[CrossRef](#)]
26. Ohmoto, H. Stable isotope geochemistry of ore deposits. In *Stable Isotopes in High Temperature Geological Processes. Rev. Mineral. Geochem.* **1986**, *16*, 491–560.
27. Hoefs, J. *Stable Isotope Geochemistry*; Springer: Berlin/Heidelberg, Germany, 2009; p. 281.
28. Zhang, L.-G.; Liu, J.-X.; Zhou, H.B.; Chen, Z.-S. Oxygen isotope fractionation in the quartz-water-salt system. *Econ. Geol.* **1989**, *89*, 1643–1650. [[CrossRef](#)]
29. Zheng, Y.F. Oxygen isotope fractionation in carbonate and sulfate minerals. *Geochem. J.* **1999**, *33*, 109–126. [[CrossRef](#)]
30. Rollinson, H.R. *Using Geochemical Data: Evaluation, Presentation, Interpretation*. Longman Scientific and Technical: London, UK, 1993; 352p.
31. Palyanova, G.A.; Savva, N.E.; Zhuravkova, T.V.; Kolova, E.E. Minerals of gold and silver in pyrites of low-sulfide ores of the Juliet deposit (North-East of Russia). *Russ. Geol. Geophys.* **2016**, *57*, 1488–1510. [[CrossRef](#)]

32. Zhuravkova, T.V.; Palyanova, G.A.; Chudnenko, K.V.; Kravtsova, R.G.; Prokopyev, I.R.; Makshakov, A.S.; Borisenko, A.S. Physicochemical models of formation of gold-silver ore mineralization at the Rogovik deposit (Northeastern Russia). *Ore Geol. Rev.* **2017**, *91*, 1–20. [[CrossRef](#)]
33. Wang, L.; Qin, K.-Z.; Song, G.-X.; Li, G.-M. A review of intermediate sulfidation epithermal deposits and subclassification. *Ore Geol. Rev.* **2019**, *107*, 434–456. [[CrossRef](#)]
34. Volkov, A.V.; Prokofiev, V.Y.; Vinokurov, S.F.; Andreeva, O.V.; Kiseleva, G.D.; Galyamov, A.L.; Murashov, K.Y.; Sidorova, N.V. Valunistoe Epithermal Au–Ag Deposit (East Chukotka, Russia): Geological structure, mineralogical–geochemical peculiarities and mineralization conditions. *Geol. Ore Depos.* **2020**, *62*, 97–121. [[CrossRef](#)]
35. Soberano, O.B.; Gabo-Ratio, J.A.S.; Queaño, K.L.; Dimalanta, C.B.; Yumul, G.P., Jr.; Andal, E.S.; Yonezu, K.; Boyce, A.J. Mineral chemistry, fluid inclusion and stable isotope studies of the Suyoc epithermal veins: Insights to Au–Cu mineralization in southern Mankayan Mineral District, Philippines. *Ore Geol. Rev.* **2021**, *131*, 104035. [[CrossRef](#)]
36. Kuzhuget, R.V.; Mongush, A.O.; Ankusheva, N.N. Sulfur sources of sulfides Of the Ak-Sug Cu–Au porphyry deposit, Eastern Tuva. *Mineralogy* **2021**, *5*, 73–81. (In Russian) [[CrossRef](#)]
37. Steele-MacInnis, M.; Lecumberri-Sanchez, P.; Bodnar, R.J. Synthetic fluid inclusions XX. Critical PTx properties of H<sub>2</sub>O–FeCl<sub>2</sub> fluids. *Geochim. Cosmochim. Acta* **2015**, *148*, 50–61. [[CrossRef](#)]
38. Berger, B.R.; Henley, R.W. Advances in understanding of epithermal gold-silver deposits with special reference to the Western United States. *Econ. Geol.* **1989**, *84*, 405–423.
39. Hedenquist, J.W.; Brown, P.R.; Allis, R.G. *Epithermal Gold Mineralization*; Applied Geology Association: Wairakei, New Zealand, 1998; 162p.
40. Vikent’eva, O.; Prokofiev, V.; Borovikov, A.; Kryazhev, S.; Groznova, E.; Pritchkin, M.; Vikentyev, I.; Bortnikov, N. Contrasting Fluids in the Svetlinsk Gold–Telluride Hydrothermal System, South Urals. *Minerals* **2020**, *10*, 37. [[CrossRef](#)]
41. Bodnar, R.J.; Beane, R.E. Temporal and spatial variations in hydrothermal fluid characteristics during vein filling in preore cover overlying deeply buried porphyry copper-type mineralization at Red Mountain, Arizona. *Econ. Geol.* **1980**, *75*, 876–893. [[CrossRef](#)]
42. Beane, R.E. The magmatic-meteoritic transition. *Geotherm. Resour. Counc. Spec. Rep.* **1983**, *13*, 245–253.
43. Reynolds, T.J.; Beane, R.E. Evolution of hydrothermal fluid characteristics at the Santa Rita, New Mexico, porphyry copper deposit. *Econ. Geol.* **1985**, *80*, 1328–1347. [[CrossRef](#)]
44. Hedenquist, J.W.; Arribas, A., Jr.; Reynolds, T.J. Evolution of an intrusion-centered hydrothermal system: Far Southeast-Lepanto porphyry-epithermal Cu–Au deposits, Philippines. *Econ. Geol.* **1998**, *93*, 373–404. [[CrossRef](#)]
45. Cooke, D.R.; Deyell, C.L.; Waters, P.J.; Gonzales, R.I.; Zaw, K. Evidence for magmatic-hydrothermal fluids and ore-forming processes in epithermal and porphyry deposits of the Baguio District, Philippines. *Econ. Geol.* **2011**, *106*, 1399–1424. [[CrossRef](#)]
46. Melfos, V.; Voudouris, P. Fluid evolution in Tertiary magmatic-hydrothermal ore systems at the Rhodope metallogenic province, NE Greece. A review. *Geol. Croat.* **2016**, *69*, 157–167. [[CrossRef](#)]
47. LeFort, D.; Hanley, J.; Guillong, M. Subepithermal Au–Pd mineralization associated with an alkalic porphyry Cu–Au deposit, Mount Milligan, Quesnel Terrane, British Columbia, Canada. *Econ. Geol.* **2011**, *106*, 781–808. [[CrossRef](#)]
48. Hedenquist, J.W.; Arribas, A.; Gonzalez-Urien, E. Exploration for epithermal gold deposits, Gold in 2000. *SEG Rev.* **2000**, *13*, 245–277. [[CrossRef](#)]
49. Voudouris, P.A. Comparative mineralogical study of Te-rich magmatic-hydrothermal systems in northeastern Greece. *Miner. Petrol.* **2006**, *87*, 241–275. [[CrossRef](#)]

**Disclaimer/Publisher’s Note:** The statements, opinions and data contained in all publications are solely those of the individual author(s) and contributor(s) and not of MDPI and/or the editor(s). MDPI and/or the editor(s) disclaim responsibility for any injury to people or property resulting from any ideas, methods, instructions or products referred to in the content.